Investigation of High-Temperature Bright Plasma X-ray Sources Produced in 5-MA X-Pinch Experiments

D. B. Sinars, R. D. McBride, S. A. Pikuz, T. A. Shelkovenko, D. F. Wenger, M. E. Cuneo, E. P. Yu, J. P. Chittenden, E. C. Harding, S. B. Hansen, B. P. Peyton, D. J. Ampleford, and C. A. Jennings

Phys. Rev. Lett. **109**, 155002 — Published 9 October 2012

DOI: 10.1103/PhysRevLett.109.155002

Investigation of high-temperature, bright plasma x-ray sources produced in 5 MA X-pinch experiments

D.B. Sinars,[1] R.D. McBride,[1] S.A. Pikuz,[2] T.A. Shelkovenko,[2] D.F. Wenger,[1] M.E. Cuneo,[1] E.P. Yu,[1] J.P. Chittenden,[3] E.C. Harding,[1] S.B. Hansen,[1] B.P. Peyton,[1] D.J. Ampleford,[1] and C.A. Jennings[1]

[1]*Sandia National Laboratories, P.O. Box 5800, Albuquerque, NM 87185, USA*

[2]*Laboratory of Plasma Studies, Cornell University, Ithaca, NY 14853, USA*

[3]*Blackett Laboratory, Imperial College, London SW7 2BW, United Kingdom*

(Dated: August 31, 2012)

Abstract

Using solid, machined X-pinch targets driven by currents rising from 0 to 5-6 MA in 60 ns, we observed bright spots of 5-9 keV continuum radiation from 5±2 μm diameter regions. The >6 keV radiation is emitted in about 0.4 ns and the bright spots are roughly 75 times brighter than bright spots measured at 1 MA. Total x-ray powers of 10 TW peak and yields of 165±20 kJ were emitted from a 3 mm height. The 3-5 keV continuum radiation had 50-90 GW peak power and 0.15-0.35 kJ yield. The continuum is plausibly from a 1275±75 eV blackbody or alternatively a 3500±500 eV bremmstrahlung source.

PACS numbers: 52.58.Lq,52.80.Qj,52.35.Py

A cylindrical current-carrying plasma can have an inward magnetic pressure from the $\vec{j}\times\vec{B}$ force exceeding its plasma pressure so that it implodes radially, or "pinches." Pinch plasmas frequently produce very brief, intense, soft x-ray bursts from tiny regions of the plasma that are variously called "bright spots," or "micropinches." Bright spots have been observed in >100 kA single-wire explosions [1], two-wire 200 kA X-pinch plasmas [2], vacuum sparks [3], plasma focus [4, 5], and wire-array z-pinches [6]. A method for reliably creating a bright spot at a predetermined location to enable it to be studied is the X-pinch configuration [7] in which two or more fine wires are arranged so that they cross at a single point. Experiments with X pinches driven by a 0.2 MA, 60-ns linearly-rising current found that micropinch plasmas can have sizes of 0.8-1.5 μm diameter [8, 9], temperatures of about 1 keV, densities >10% of solid density, and durations of 10-100 ps [2, 10, 11]. These high energy density plasmas have a plasma pressure of about 0.4 Gbar, comparable to the 1-Gbar magnetic pressure of 0.2 MA at 1 μm.

Understanding micropinch plasmas is important. For example, 16 MA tungsten wire-array z-pinch experiments contain numerous small, brightly emitting regions in 6.15 keV emission that may emit about 30% of the total 1 MJ 0.1-10 keV radiation yield [12], including most of the >2 keV radiation. Data from 0.2 MA X-pinch experiments has been explained using a model based on approximate Bennett equilibrium conditions in which a balance was achieved between blackbody radiation losses and Joule (thermal) heating by the current [13]. Assuming the collapse ends at a radius of 1 μm, this equilibrium model predicts a ten-times-solid density, 156 Gbar plasma at 1 MA! Recent experiments studied multi-wire X-pinch loads at currents up to 2.3 MA, reporting spot size measurements down to about 20 μm and measured radiation powers of 120 GW in 1-3 keV radiation [14, 15], but testing the predictions of Ref. 13 requires more detailed data.

Here we summarize results from 31 X-pinch experiments on the 6 MA, 60-ns SATURN pulsed power facility in which we directly measured several key bright spot parameters for the first time for currents up to 5 MA. The SATURN experiments extend previous work on the 1 MA, 100-ns COBRA facility [16]. We fielded several X-pinch load designs that were first evaluated on 1 MA experiments, including large wire-number cylindrical wire arrays twisted into an X-pinch [16], nested multi-layered wire arrays twisted into an X-pinch [17], and a hybrid configuration in which a single wire is strung across two conical electrodes [16, 18, 19]. However, most of our SATURN experiments used X-pinch loads with solid,

machined cross points as shown in Fig. 1. The targets were made of tungsten, a W/Cu alloy (47.1/52.9 atomic %), or a Cu/Ni/Mn alloy (53/45.9/1.1 atomic %) with minimum mass per unit length values in the12-24 mg/cm range. These masses were chosen based on the self-similar implosion scaling law [20], $\Pi = (\mu_0 I^2 \tau^2)/(4\pi m_l r^2)$, where Π is a scaling constant, I is the peak current, τ is the implosion time, m_l is the liner mass per unit length, and r is the radius. Increasing the radius is the only way to vary m_l for solid density, on-axis matter, so that m_l scales linearly with current. Previous experiments at 1 MA were about 3 mg/cm [16].

Example current and radiation traces are plotted in Fig. 2. The current in these experiments was measured using B-dot probes located upstream of the load [21]. The first significant >3 keV x-ray burst typically occurred at current values ranging from 3-5 MA. As described previously [16], the total soft x-ray power was measured using x-ray diodes normalized to Ni bolometers, and photoconducting diodes (PCDs) filtered with 25 μm Be or 12 μm Ti measured >1 keV and 3-5 keV continuum radiation, respectively. Typical peak radiation powers were about 10 TW (total emission), 200-500 GW (>1 keV), and 15-90 GW (3-5 keV). Typical x-ray yields were 100-150 kJ (total), 1-5 kJ (>1 keV), and 50-300 J (3-5 keV). The best radiating material was tungsten, which had total x-ray powers of 10 TW peak and yields of 165±20 kJ, and 3-5 keV radiation of 50-90 GW peak power and 150-350 J yield.

The diodes were sampled every 200 ps, which could lead to underestimates of the power for source durations <100 ps. On a limited number of tests we used an x-ray streak camera to obtain continuous time resolution. The camera photocathode was about 7 m from the target with the same 35° view as the diodes. In the example data shown in Fig. 3, a short burst with strong >5 keV x-ray emission is seen followed by a series of weaker bursts. The streak image shows more discrete structure than the corresponding PCD trace shown in Fig. 2. About one quarter of the width of the pulses in Fig. 3a is due to the streak response (the static slit image is about 100 ps wide). Deconvolving this width from the data gives a full-width-at-half-maximum for the >5 keV emission of about 0.4 ns. If the streak camera was out of focus (a recurring problem here), the duration could be shorter.

The relative streak camera response from 1-30 keV, shown in Fig. 3b, was determined using the transmission of the various filters [22] with a model for the back-surface quantum yield of the 102-Å Au photocathode [23]. The image in Fig. 3a was processed to find

the relative signal amplitudes for the first x-ray burst through each of six different filters (Fig. 3c). These data are compared with blackbody and bremsstrahlung models for the continuum radiation. Since the absolute response of the streak camera is unknown, the model results were normalized to match the total amplitude of the six data signals. Clearly to distinguish between the two models it would have been desirable to obtain data at >10 keV, but the streak camera did not have a sufficient dynamic range to permit this. A range of temperatures give similar fits to the data. Above and below these ranges the relative amplitudes of the low- and high-energy filter groupings disagree with the data. The slope of the 5-10 keV continuum measured using a time-integrated spectrometer on W and W/Cu experiments is also consistent with the slope implied by this time-resolved streak data. In Cu/Ni/Mn experiments we saw strong K-shell radiation from Cu, Ni, and Mn, implying few keV electron temperatures. The Cu radiation was suppressed and the continuum stronger in W/Cu experiments, consistent with the higher efficacy of tungsten X-pinches at converting electrical energy into radiation.

The source size in soft x rays was found using time-gated multi-layer mirror pinhole cameras [24]. Example monochromatic (277 eV) and broadband (>1 keV) x-ray images are shown in Fig. 4. The 277 eV data is representative of the total soft x-ray power data, and as in Fig. 4a this emission was always observed from a roughly 3 mm (or less) vertical region on solid-target X-pinch tests. The keV image was generally smaller, particularly during the first x-ray burst. In 0.2 MA experiments the first x-ray burst is associated with the smallest x-ray source sizes, and later x-ray bursts are associated with a subsequent disruption of the pinch plasma as verified in radiography data [25]. We note that the best thermal radiation sources on SATURN are 20 mm tall W wire arrays that produce 75±10 TW and 450±50 kJ, for about 4 TW/mm and 23 kJ/mm [26]. The 10 TW and 165±20 kJ made by our W X-pinch sources are comparable at roughly 3 TW/mm and 55 kJ/mm. This is interesting because unlike a cylindrical wire array, which involves a high-velocity implosion of mass to the array axis, all of the X-pinch mass starts on axis and the implosion kinetic energy remains low.

The time-integrated multi-keV source size was inferred with high spatial resolution using an array of 20-, 40-, and 80-μm wide slits at a distance of 100 mm horizontally from the target and a detector at 660 mm. As was done previously [8, 16], wave-optics modeling is used to calculate slit images for different source sizes. Only x-ray sources $\leq$9 μm in

diameter project slit images with equal peak intensities at all three slit sizes. For $\leq$3 μm sources, diffraction peaks become visible. Example data is shown in Fig. 5 that is consistent with a time-integrated 6-9 keV source size of 5 μm diameter. The slit measurements were very difficult to obtain due to background from high-energy diffuse sources (e.g., post-pinch electron beams [27, 28]), so only some tests succeeded in this direct measurement.

A key question is whether the bright spots in our 5 MA experiments correspond to more extreme states of matter than observations from 0.2-1 MA experiments. We first note that the total 3-5 keV radiation power and energy from our 5 MA W X-pinch experiments are much higher than the $\sim$2 J, 1-10 GW measured in 1 MA W X-pinch experiments [16] using the same techniques. Second, in some SATURN experiments the same slits, filters, and similar films and magnification (about 6) were used as in our 1 MA experiments. The main difference was that the slits were located 1188 mm from the target instead of 137 mm, for a difference in solid angle of about 75. Comparable film exposures were seen in both experiments in both Cu- and Ti-filtered slit images, a direct measurement that the bright spots are roughly $\sim$75 times brighter.

Third, there is self-consistency in the measured radiation power, the measured source size, and the inferred blackbody spectrum implied by the analysis in Fig. 3. A 1275 eV (brightness temperature) blackbody emits 2.7e21 W/m^2 in the 0.05-30 keV range. About 6e20 W/m^2 of this passes through a 12.5 μm Ti filter, so that a Ti-filtered PCD would measure roughly 4.3 times less than the total radiated power from the blackbody. Assuming a 1275 eV blackbody source implies that the $\sim$90 GW measurements of Fig. 2b correspond to 0.4 TW of total radiation out of the $\sim$10 TW in Fig. 2a, a reasonable fraction with the remainder presumably coming from the larger surrounding plasma seen in Fig. 4. This assumption further implies a surface area of 1.4e-10 m^2, corresponding to a 6.6 μm diameter for a spherical surface and consistent with the measurements in Fig. 5.

Finally, blackbody X-pinch sources are theoretically plausible. We ran three-dimensional radiation magneto-hydrodynamic simulations of a tungsten X-pinch on SATURN using the GORGON code [13], using 1.6 μm resolution and random single-cell surface perturbations. As shown in Fig. 6, after an initial shock a partly quasi-static compression phase follows during which significant axial mass redistribution occurs and instabilities rapidly develop. As in 200 kA experiments [25] the necks "cascade, consistent with SATURN observations of both large, long-duration sources and multiple small bright spots. The radial compression

is enabled in part by axial mass flow, but the cross-point region remains dense throughout the implosion. This simulation radiated about 4.5 TW at peak power in a near-blackbody spectrum, mainly from the narrow necks. The conditions at this time are extreme, with ∼200 Gbar thermal pressures and magnetic pressures a few times that, for peak fields of about 150,000 T and peak densities >400 g/cm^3.

Calculated emission spectra assuming a 6 μm diameter, 1.3 keV plasma indicate that densities more than five times solid would be required for the bright-spot emission to be consistent with our streak data, peak radiated power, and time-integrated W/Cu spectra. For higher plasma temperatures of about 3 keV, near-solid densities would be consistent with our data. Densities from 1-10 times solid are significantly higher than those inferred for lower-current bright spots, but they do not reach the extreme conditions predicted in Ref. 13.

Our data clearly show remarkable results from 5 MA X-pinch experiments, and clearly indicate more extreme bright spot parameters such as power and brightness have been achieved than those from lower-current experiments. Without a better density measurement it is difficult to say what the plasma pressure of our x-ray sources is. An alternative might be to measure the magnetic field associated with the extreme magnetic pressures predicted by simulations. At the ∼100,000 T fields generated by MA currents at few μm diameters, Zeeman splitting on the order of tens of eV may be observable in x-ray emission lines, provided that we could overcome density broadening [29]. We hope our data will help to motivate future experiments along these lines.

We thank Dr. Mark Herrmann for his encouragement, the SATURN operations crew for experimental support, Linda Nielsen for film support, and the Z load hardware team for hardware support. The project was funded in part by Sandia's Laboratory Directed Research and Development program. Sandia National Laboratories is a multi-program laboratory managed and operated by Sandia Corporation, a wholly owned subsidiary of Lockheed Martin Corporation, for the U.S. Department of Energy's National Nuclear Security Administration under contract DE-AC04-94AL85000.

[1] P. G. Burkhalter, C. M. Dozier, and D. J. Nagel, Phys. Rev. A **15**, 700 (1977).

[2] S. A. Pikuz *et al.*, Phys. Rev. Lett. **89**, 035003 (2002).

[3] K. N. Koshelev and N. R. Pereira, J. Appl. Phys. **69**, R21 (1991).

[4] B. A. Trubnikov, Sov. J. Plasma Phys. **12**, 271 (1986).

[5] V. V. Vikhrev, Sov. J. Plasma Phys. **12**, 262 (1986).

[6] N. R. Pereira and J. Davis, J. Appl. Phys. **64**, R1 (1988).

[7] S. M. Zakharov *et al.*, Sov. Tech. Phys. Lett. **8**, 456 (1982).

[8] B. M. Song, S. A. Pikuz, T. A. Shelkovenko, and D. A. Hammer, Appl. Opt. **44**, 2349 (2005).

[9] T. A. Shelkovenko *et al.*, Rev. Sci. Instrum. **72**, 667 (2001).

[10] D. B. Sinars *et al.*, J. Quant. Spectrosc. Radiat. Transfer **78**, 61 (2003).

[11] S. B. Hansen *et al.*, Phys. Rev. E **70**, 026402 (2004).

[12] D. B. Sinars *et al.*, Phys. Rev. Lett. **100**, 145002 (2008).

[13] J. P. Chittenden *et al.*, Phys. Rev. Lett. **98**, 025003 (2007).

[14] S. S. Anan'ev *et al.*, JETP Lett. **87**, 364 (2008).

[15] S. S. Anan'ev *et al.*, Plasma Phys. Rep. **35**, 459 (2009).

[16] D. B. Sinars *et al.*, Phys. Plasmas **15**, 092703 (2008).

[17] T. A. Shelkovenko *et al.*, Phys. Plasmas **16**, 050702 (2009).

[18] T. A. Shelkovenko *et al.*, Phys. Plasmas **17**, 112707 (2010).

[19] T. A. Shelkovenko *et al.*, Plas. Phys. Rep. **38**, 359 (2012).

[20] D. D. Ryutov, M. S. Derzon, and M. K. Matzen, Rev. Mod. Phys. **72**, 167 (2000).

[21] T. C. Wagoner *et al.*, Phys. Rev. Spec. Topics Accel. and Beams **11**, 100401 (2008).

[22] B. L. Henke, E. M. Gullikson, and J. C. Davis, Atomic Data Nucl. Data Tab. **54**, 181 (1993).

[23] B. L. Henke, J. P. Knauer, and K. Premaratne, J. Appl. Phys. **52**, 1509 (1981).

[24] B. Jones *et al.*, Rev. Sci. Instrum. **79**, 10E906 (2008).

[25] T. A. Shelkovenko, D. B. Sinars, S. A. Pikuz, and D. A. Hammer, Phys. Plasmas **8**, 1305 (2001).

[26] C. Deeney *et al.*, Phys. Rev. E **56**, 5945 (1997).

[27] V. L. Kantsyrev *et al.*, Phys. Plasmas **10**, 2519 (2003).

[28] T. A. Shelkovenko *et al.*, Plas. Phys. Rep. **34**, 754 (2008).

[29] E. Stambulchik, K. Tsigutkin, and Y. Maron, Phys. Rev. Lett. **98**, 225001 (2007).

FIG. 1: Half-section drawing of the hardware. A solid, machined cross-point of the desired material is inserted between two tungsten electrodes as the load of the SATURN facility. Most diagnostics had a 35° view below the horizontal.

FIG. 2: Example data from selected X-pinch tests. (a) Total load current and the total soft x-ray power. (b) 3-5 keV x-ray power measured using a PCD with a 12.5 μm Ti filter.

FIG. 3: X-ray streak camera data from a W/Cu X-pinch test (s3859). (a) Time-calibrated streak image. The (slightly tilted) photocathode slit was covered with 12.7 μm Kapton (polyimide) and ten additional filters of different materials and thicknesses to provide spectral information. An additional 125 μm Kapton debris filter was also used. Accounting for the width of the static slit image, the data are consistent with a 0.4 ns main pulse duration. (b) Plot of the net streak camera response as a function of photon energy compared with two models for the continuum emission. (c) Comparison of measured and calculated signal amplitudes for six of the streak filters, using two different emission models. The data error bars represent film signal variations after background subtraction. The modeling error bars represent variations due to $\pm$0.5 μm filter thickness uncertainties. Similar quality matches to the data are obtained for blackbody temperatures 1275$\pm$75 eV and bremsstrahlung temperatures 3500$\pm$500 eV.

FIG. 4: Time-gated multi-layer mirror pinhole camera images (4 mm by 4 mm, 3-ns gate times) from a Cu/Ni X-pinch test (s3812). (a) Monochromatic 277 eV image data ($\sim$0.5 mm resolution). (b) Broadband >1 keV image data (8-μm Be filter, $\sim$0.2 mm resol.). (c) Solid model view of initial cross-point for comparison. (d) Plot of the soft (XRD) and hard (PCD) x-ray power from the experiment. The cross-timing of each MLM row and each diode is accurate to $\pm$1.5 ns.

FIG. 5: Time-integrated slit camera data (40 μm Cu filter) from a W X-pinch test (s3941). (a) A portion of the film image. Three offset x-ray sources produced sharp and diffuse projections of each of the 20, 40, and 80-μm slits. (b) Lineouts along the two regions from part (a). (c) The difference of the two lineouts from part (b). Vertical black bars of the same size are overlaid to illustrate that the three slit images have the same peak amplitude. (d) Simulated lineouts for a 20 μm slit calculated using wave-optics modeling assuming source sizes from 3 to 20 μm, overlaid with the normalized data from part (c). (e) The same for the 40 μm slit. The data are most consistent with a source size of 5$\pm$2 μm.

FIG. 6: Log density (kg/m^3) slices through 3D MHD simulations of a solid W X-pinch experiment. The times shown are relative to peak x-ray emission. The structure mostly remains cylindrically symmetric because of the large on-axis mass but the density and pressure at peak compression are limited by 3D asymmetry.

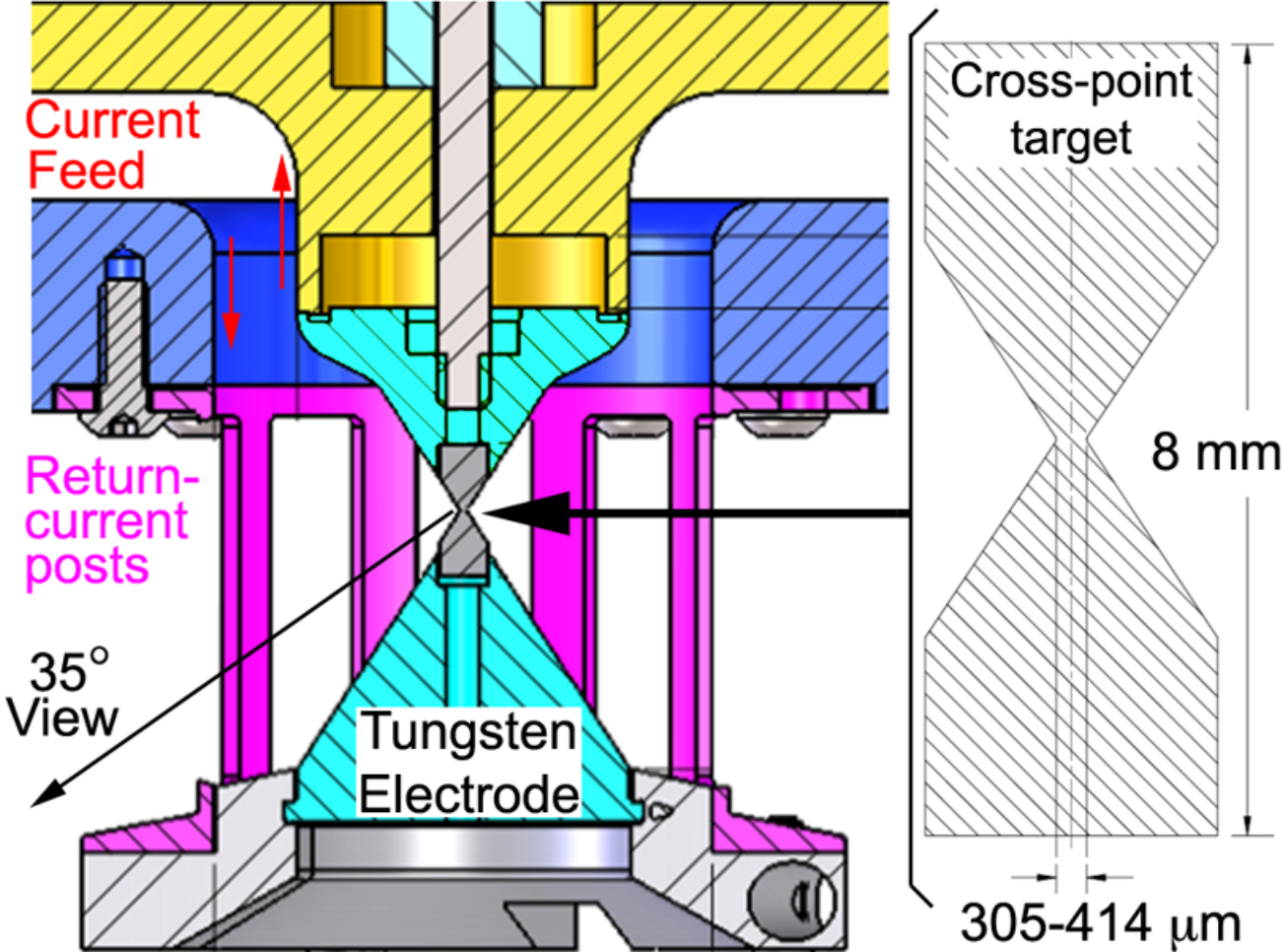
Current
Feed
Return-
current
posts
35°
View
Tungsten
Electrode
Cross-point
target
8 mm
305-414 μm

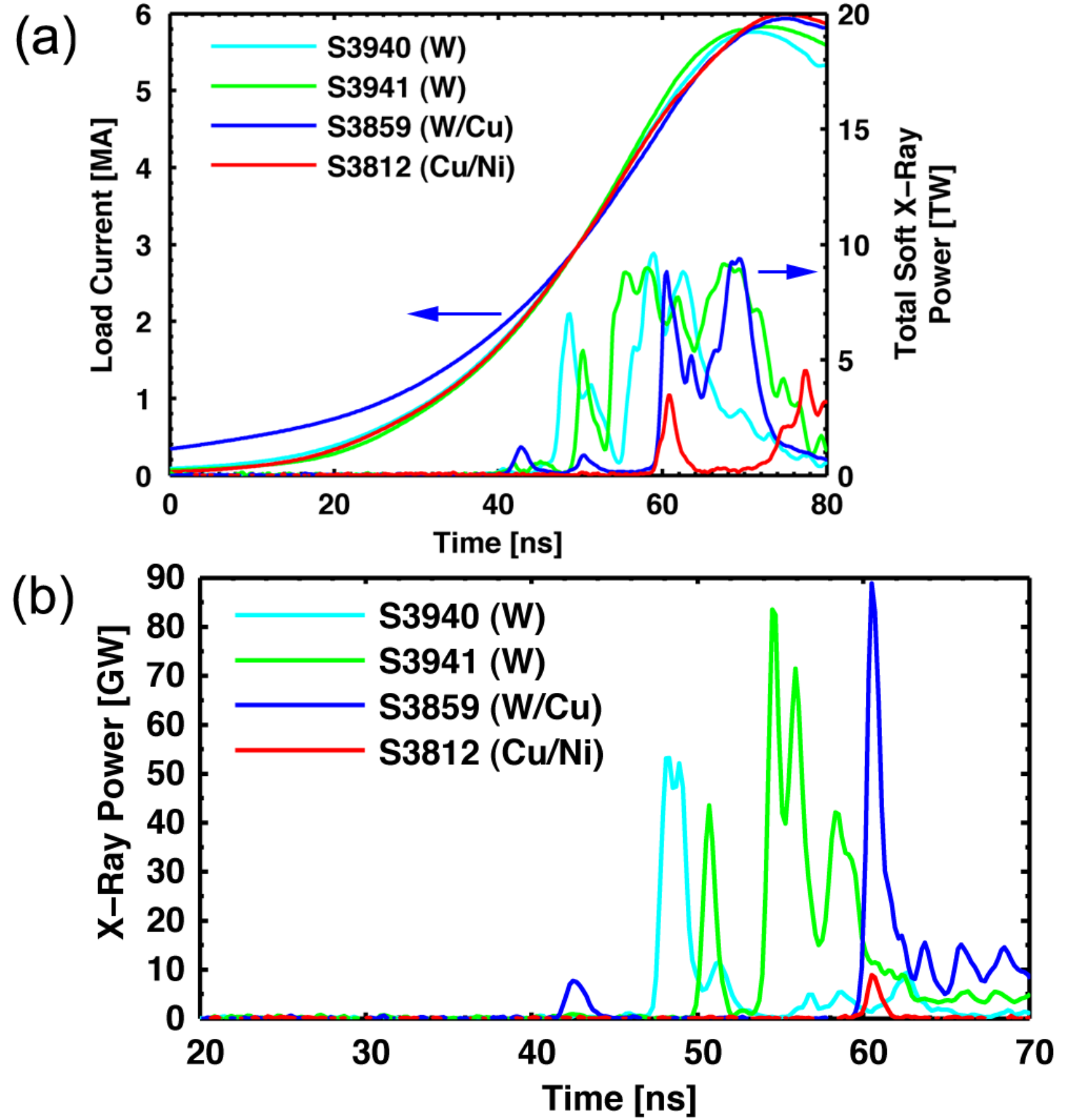
(a)
S3940 (W)
S3941 (W)
S3859 (W/Cu)
S3812 (Cu/Ni)
Load Current [MA]
Total Soft X–Ray Power [TW]
Time [ns]
0
1
2
3
4
5
6
0
5
10
15
20
0
20
40
60
80
(b)
S3940 (W)
S3941 (W)
S3859 (W/Cu)
S3812 (Cu/Ni)
X–Ray Power [GW]
Time [ns]
0
10
20
30
40
50
60
70
80
90
20
30
40
50
60
70

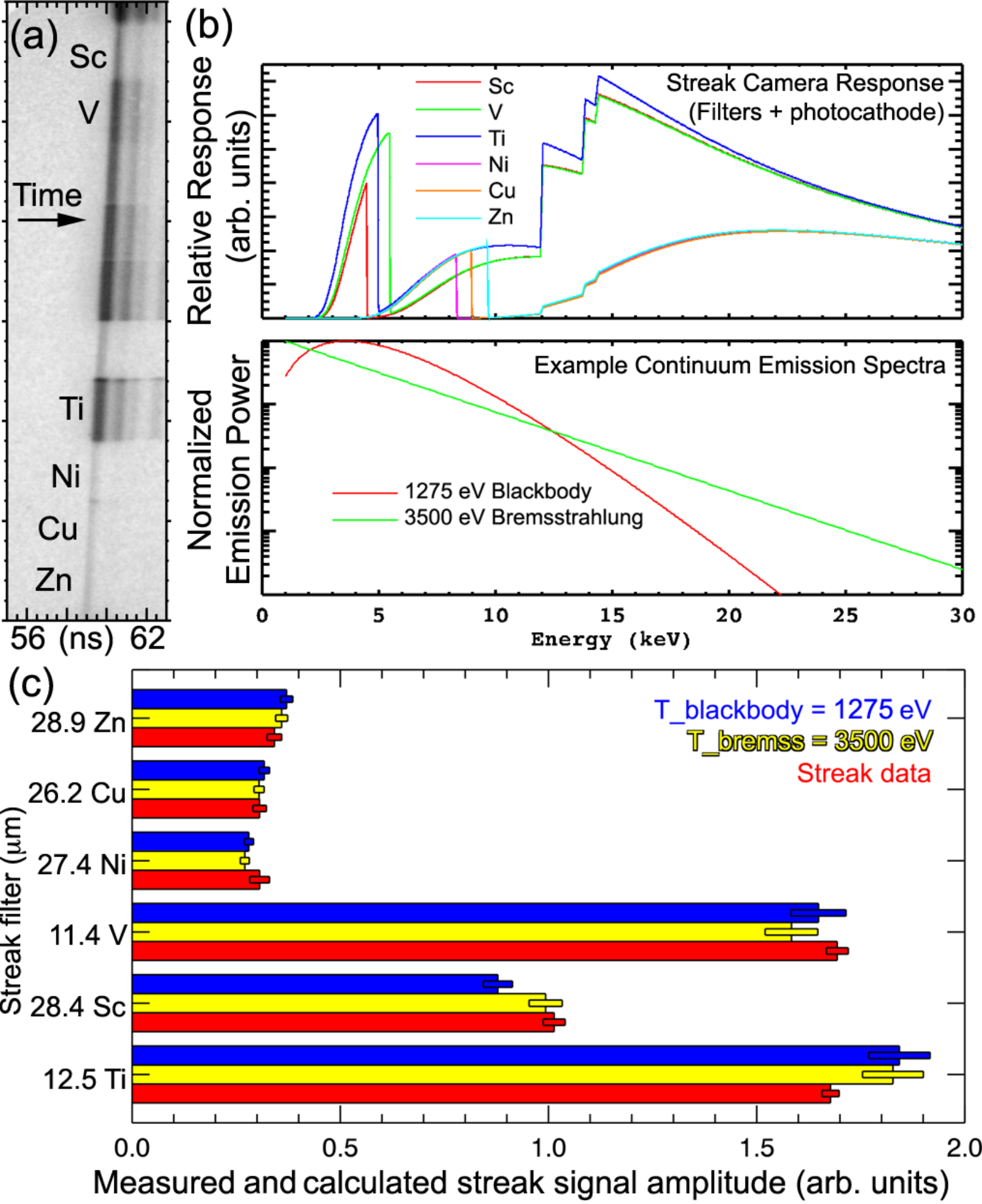
(a)
Sc
V
Time
Ti
Ni
Cu
Zn
56 (ns) 62
(b)
Relative Response (arb. units)
Sc
V
Ti
Ni
Cu
Zn
Streak Camera Response
(Filters + photocathode)
Normalized Emission Power
Example Continuum Emission Spectra
1275 eV Blackbody
3500 eV Bremsstrahlung
0
5
10
15
20
25
30
Energy (keV)
(c)
T_blackbody = 1275 eV
T_bremss = 3500 eV
Streak data
Streak filter (μm)
28.9 Zn
26.2 Cu
27.4 Ni
11.4 V
28.4 Sc
12.5 Ti
0.0
0.5
1.0
1.5
2.0
Measured and calculated streak signal amplitude (arb. units)

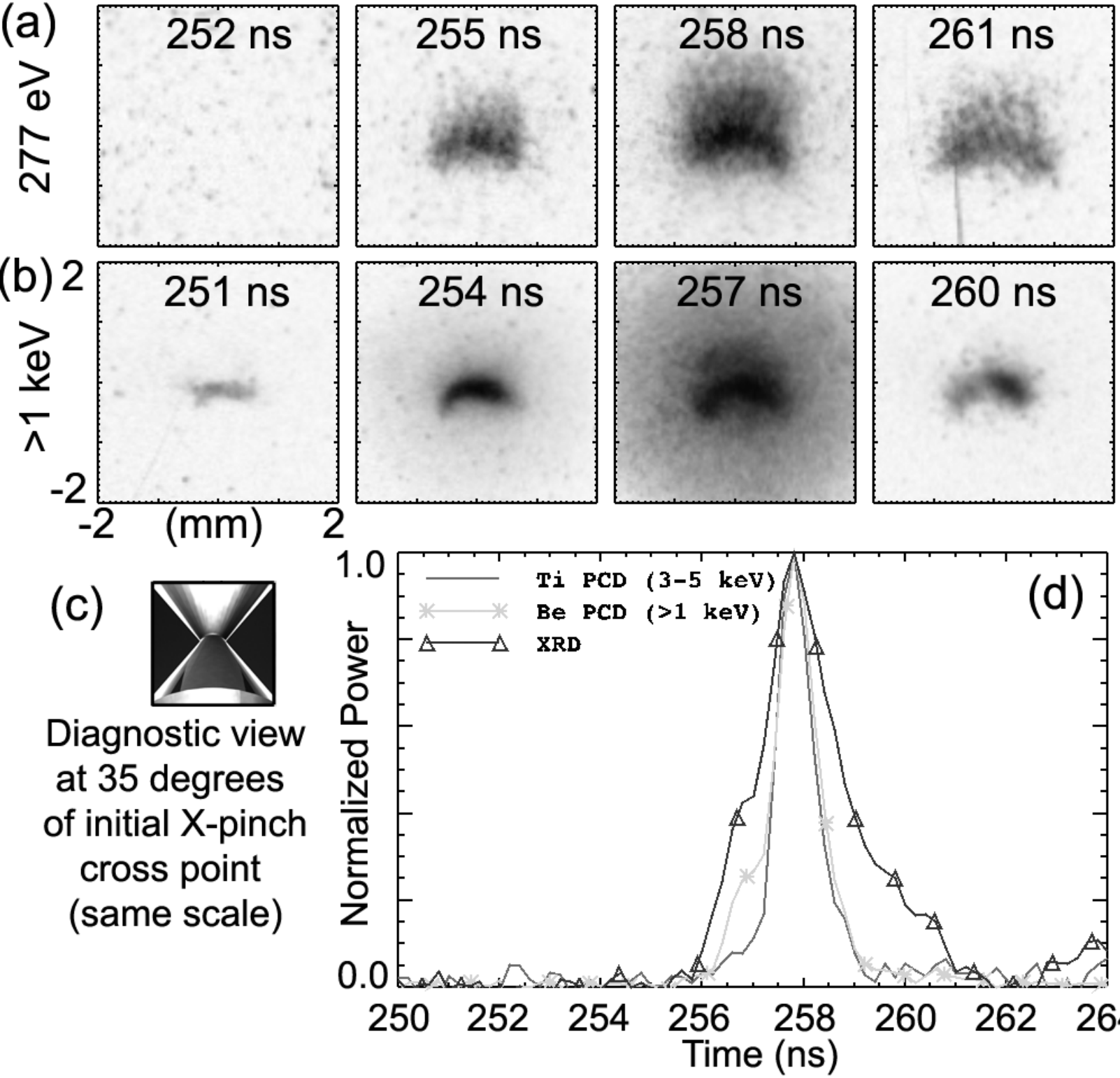
(a)
277 eV
252 ns
255 ns
258 ns
261 ns
(b)
>1 keV
2
-2
251 ns
254 ns
257 ns
260 ns
-2
(mm)
2
(c)
Diagnostic view at 35 degrees of initial X-pinch cross point (same scale)
(d)
Ti PCD (3-5 keV)
Be PCD (>1 keV)
XRD
Normalized Power
1.0
0.0
250
252
254
256
258
260
262
264
Time (ns)

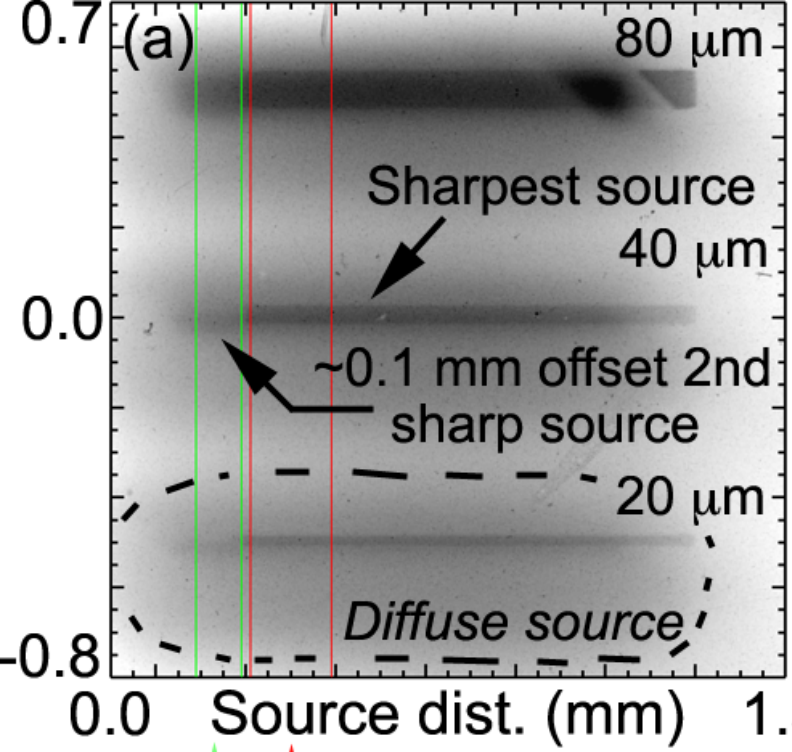

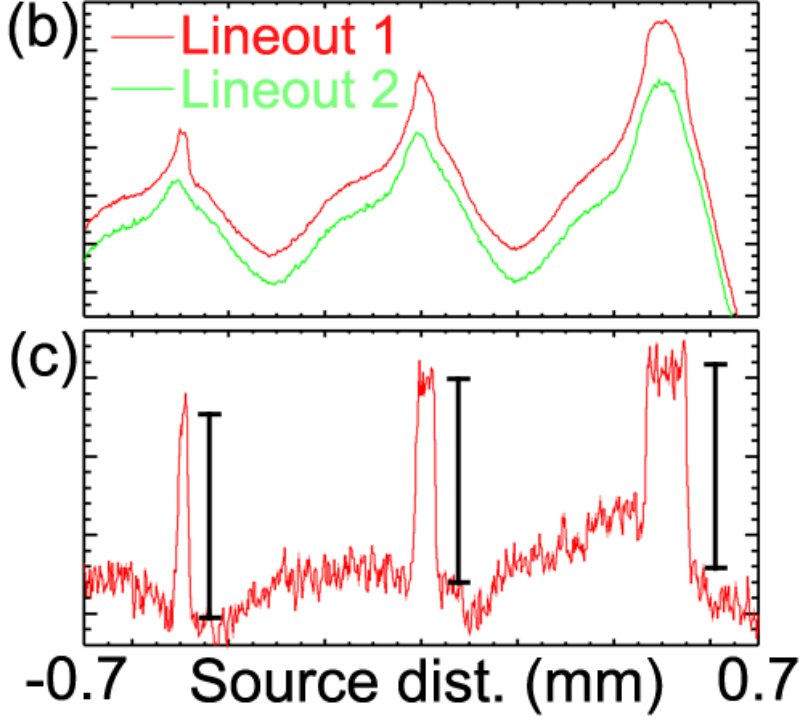

Horizontally-averaged vertical lineouts

Lineout 1 includes all three sources (2 sharp, 1 diffuse)

Lineout 2 doesn't include sharpest source

Difference of two lineouts yields only contribution from sharpest source

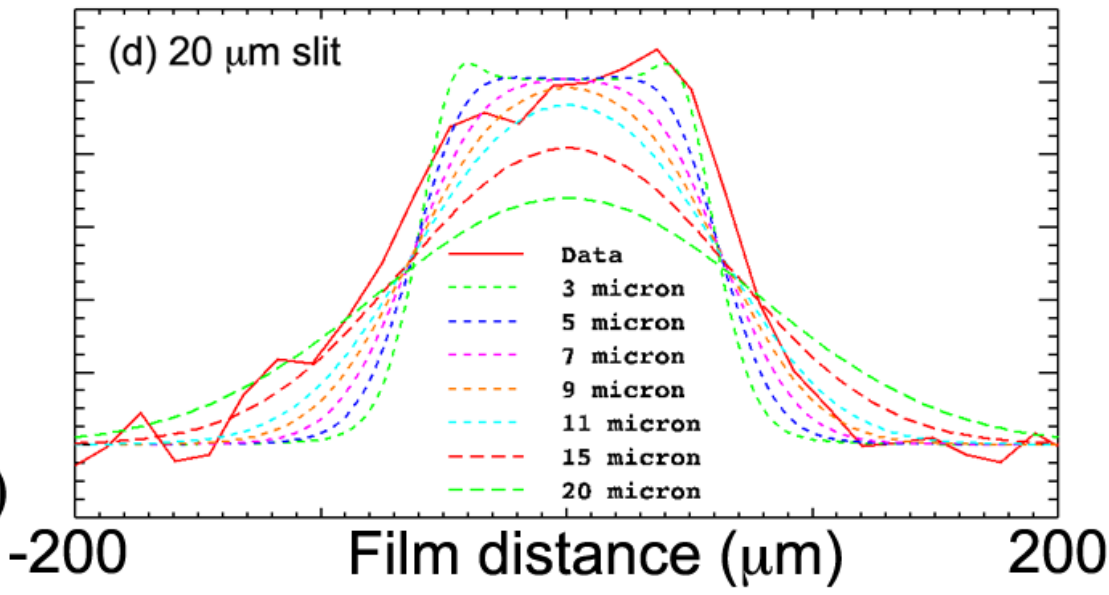

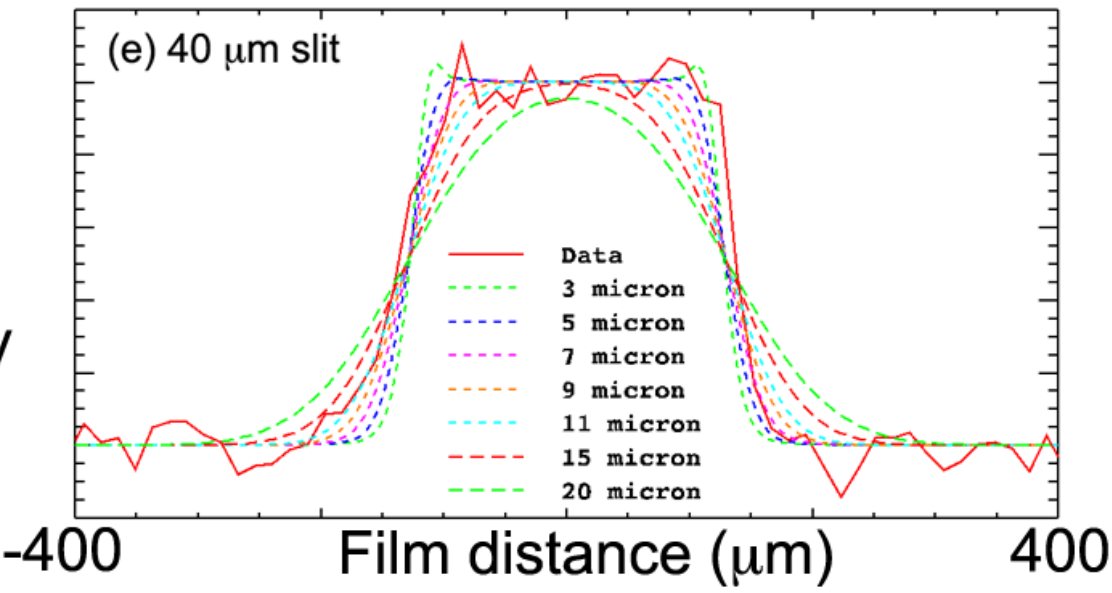

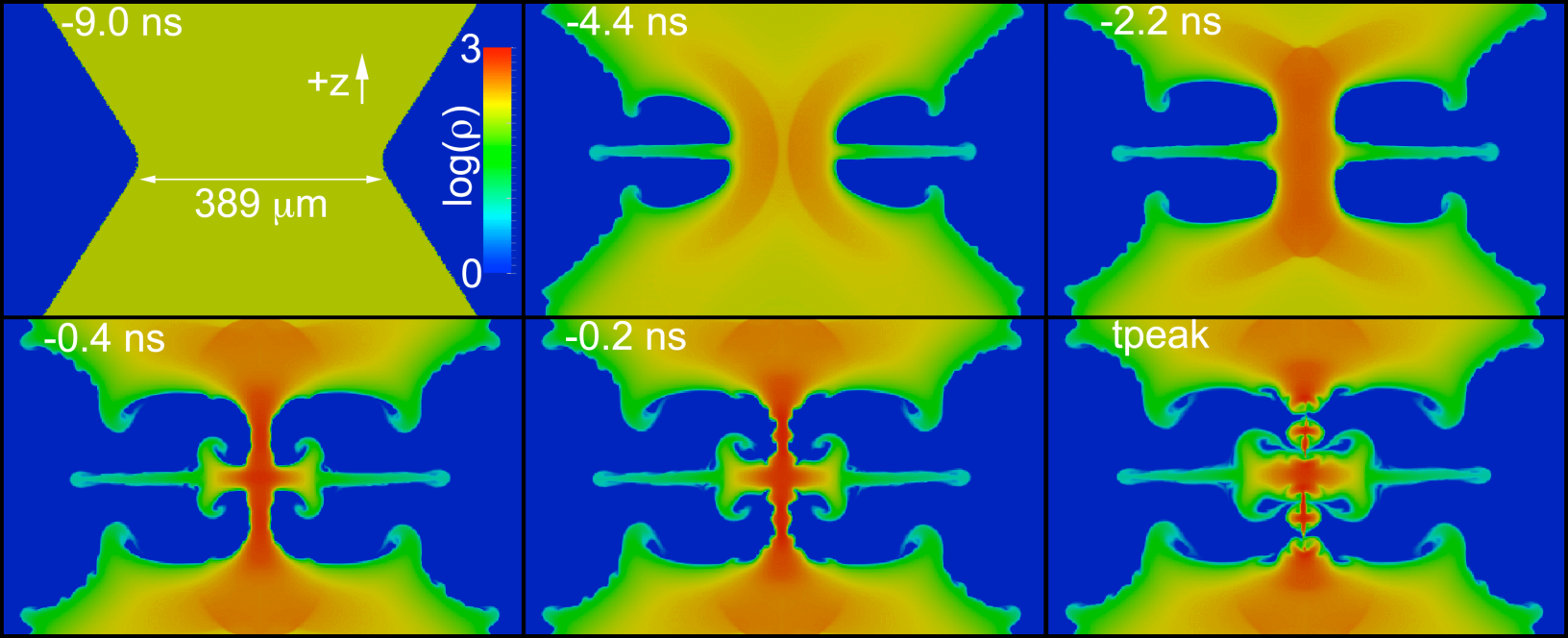
-9.0 ns
+z
389 μm
log(ρ)
3
0
-4.4 ns
-2.2 ns
-0.4 ns
-0.2 ns
tpeak